Interaction Notes

Note 221

January 1975

FIELD PENETRATION INTO A CYLINDRICAL CAVITY

T. B. A. Senior
The University of Michigan Radiation Laboratory
Department of Electrical and Computer Engineering
Ann Arbor, Michigan 48104

Abstract

To test the efficacy of a direct integral equation approach to the study of cavity-aperture interactions, the problem of an E-polarized plane electromagnetic wave incident on a thin, perfectly conducting cylindrical shell with a slit aperture is considered. A computer program is constructed for the solution of the appropriate E field integral equation. Data are presented showing the behavior of the field inside the cavity and in the aperture for a variety of aperture and cavity dimensions, and some information is obtained about the SEM singularities and their dependence on aperture size.

SECTION I

INTRODUCTION

The present study was motivated by some recent investigations of the coupling of an electromagnetic field into a spherical cavity. In the particular case when the cavity is bounded by a thin, perfectly conducting shell having a circular aperture, it is not unnatural to expand the interior and exterior fields in spherical modes, and as shown in ref. 1 it is then possible to calculate the fields inside the cavity. Unfortunately, there are difficulties, most of which are attributable to the poor convergence of the interior mode expansions in the vicinity of the boundary. These have been discussed by Senior (ref. 2) who has proposed instead an alternative formulation based on the E field integral equation for the total current induced in the shell. The resulting coupled integral equations for the tangential components of the current appear quite amenable to solution by the moment method, and are also convenient for the numerical determination of the complex frequency singularities of the singularity expansion method (SEM).

In order to demonstrate the efficacy of this approach, we here consider the simpler two-dimensional problem of a plane wave incident on a thin, perfectly conducting, cylindrical shell having a slit aperture. In most respects, this problem is physically and mathematically akin to the spherical one, and our original interest was to pursue the solution only far enough to verify that there are no difficulties involved. Nevertheless, the problem does have interest in its own right, and data have been obtained for the currents, aperture and interior fields for a variety of aperture angles and ka in the range $0.25 \leq ka \leq 4.0$ where ka is the electrical circumference of the (closed) cylinder. Selected data are presented in Section III, along with information about the first few complex singularities and their dependence on aperture size. A description and print-out of the computer program are included as an Appendix.

SECTION II

MATHEMATICAL FORMULATION

A thin, perfectly conducting cylindrical shell of radius a having a slit aperture of half angle ϕ_o is illuminated by an E-polarized plane wave incident in a plane perpendicular to the z axis of the cylinder. In terms of the polar coordinates (ρ, ϕ, z) the equation of the shell is $\rho = a$, $\phi_o \leq \phi \leq 2\pi - \phi_o$, and the incident electric field is taken to be

$$\underline{E}^i = \hat{z}\, e^{-ik\rho\cos(\phi - \alpha)} \tag{1}$$

(see Figure 1), where a time factor $e^{-i\omega t}$ has been assumed and suppressed.

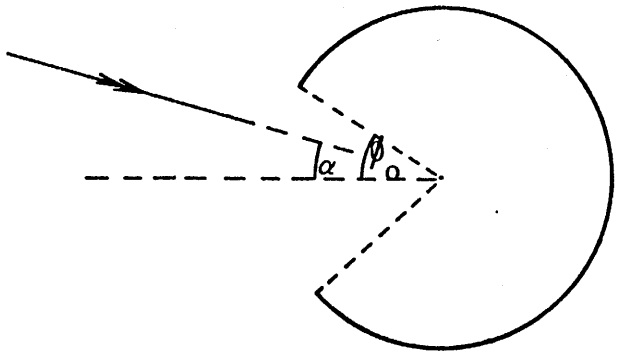

Figure 1. The Geometry

Since the shell is infinitesimally thin, it can be represented by an electric current sheet of strength $J_z(s')$, where $\underline{J}(s') = \hat{z}\, J_z(s')$ is the total current borne by the shell. The scattered electric field at a point having the position vector $\underline{\rho}$ is then

$$\underline{E}^s(\rho) = -\hat{z}\frac{kZ_o}{4}\int_C J_z(s')\,H_o^{(1)}(kR)\,ds' \qquad (2)$$

where $Z_o = 1/Y_o$ is the intrinsic impedance of free space, $H_o^{(1)}$ is the Hankel function of the first kind and R is the distance between the integration and observation points. The integration is along the shell ('one side' only) in the plane perpendicular to the z axis containing the observation point, and consequently $s' = a\phi'$ with $\phi_o \leq \phi' \leq 2\pi - \phi_o$.

The total field is obtained by adding (1) and (2), and if we now allow the observation point to lie on the shell and use the boundary condition at a perfect conductor, the following integral equation results:

$$Y_o e^{-ika\cos(\phi-\alpha)} = \frac{ka}{4}\int_{\phi_o}^{2\pi-\phi_o} J_z(\phi')\,H_o^{(1)}(kR)\,d\phi' \quad . \qquad (3)$$

This is merely a special case of an integral equation for resistive sheets previously considered by Knott et al (ref. 3), and a computer program for its solution is described in the Appendix to this report. Having found the current J_z, the field at any point can be calculated from eqs. (1) and (2). We note in passing that for an H-polarized incident plane wave, the integral equation for the total current induced in the shell is more complicated than (3), but a rather general computer program with which its solution can be obtained is available (ref. 4).

In contrast to the mode-matching method used by Senior and Desjardins (ref. 1) in the solution of the corresponding problem for a sphere, the direct integral equation approach is convenient for the calculation of the complex frequency (SEM) singularities, and the determination of their dependence on aperture size. For the interior region $\rho \leq a$, the cylindrical mode expansion has the form

$$\sum_{n=-\infty}^{\infty} a_n J_n(k\rho)\,e^{in\phi} \quad ,$$

and if the cavity were closed, the singularities would be the real resonant frequencies corresponding to the zeros of $J_n(ka)$, i.e.

$$\omega = u_{mn}\, c/a$$

where u_{mn} is the m^{th} zero of $J_n(u)$. When ordered in increasing magnitude, the first few are

$$\begin{aligned} \omega &= 2.405\ c/a && (m=1,\ n=0) \\ &= 3.832\ c/a && (m=1,\ n=1) \\ &= 5.136\ c/a && (m=1,\ n=2) \\ &= 5.520\ c/a && (m=2,\ n=0)\ . \end{aligned}$$

Each has its counterpart in the case of a spherical cavity, and the first two are even similar in magnitude to those for a sphere. If the slit is now opened, the complex frequencies must take on a negative imaginary part associated with the radiation damping of the modes, and in addition it is expected that the real parts will decrease with increasing aperture size.

The exterior region $\rho \geq a$ is rather different. The cylindrical mode expansion here is

$$\sum_{n=-\infty}^{\infty} b_n\, H_n^{(1)}(k\rho)\, e^{in\phi}\ ,$$

and for a complete perfectly conducting cylinder the complex frequencies are

$$\omega = v_{mn}\, c/a$$

where v_{mn} is the m^{th} zero of $H_n^{(1)}(v)$. The nature of these zeros is discussed in ref. 5 (see also ref. 6), and the zero with the smallest imaginary part is

$$v_{10} = -2.404 - i0.3405.$$

In addition, there is a branch point at $\omega = 0$, which has no counterpart in the case of a finite body.

SECTION III

NUMERICAL RESULTS

With the aid of the computer program described in the Appendix, the integral equation (2) has been solved to give data for the fields inside the cavity and in the aperture, as well as some information about the complex frequency singularities. No difficulties have been experienced in any of the more than 100 individual runs that have been made so far. Although many of these runs have been directed at the complex frequency singularities, with the program interrupted following the computation of the determinant, it is evident that only a small selection of the data can be presented here. For the data which follow, the number of sampling points used was increased almost linearly with ka, from a minimum of 12 for $ka \leq 1.0$ to a maximum of 48 for $ka \geq 3.5$. The largest ka considered was 4.0, and most attention was directed at cavities having aperture half-angles $\phi_o = 10^o$ and 30^o with the plane wave at symmetrical incidence, i.e. $\alpha = 0$.

The amplitudes of the total currents $J_z(\phi)$ induced in the shell are illustrated in Figures 2 through 5. Since $\alpha = 0$, the currents are symmetrical about $\phi = 180^o$, and only the ranges $\phi_o \leq \phi \leq 180^o$ are displayed. As expected, the currents are infinite at $\phi = \phi_o$. The curves become increasingly complex as ka increases, and we note the enhanced values of $|J_z|$ for $\phi_o = 30^o$ when ka = 2.3, i.e. close to the first resonant frequency of the cavity. The amplitudes of the corresponding aperture fields are shown in Figures 6 through 9. The fields are zero at $\phi = \pm\phi_o$ in accordance with the edge condition, and in contrast to the shell currents, the aperture fields are rather simply behaved. This is in line with the observation in ref. 1 , though we note that even for $\phi_o = 30^o$ and ka = 4.0, the aperture is still only 0.67λ in width. The fields are a maximum at the first resonant frequency of the cavity, but very small at the next (ka = 3.83), and the variation with frequency is brought out in Figure 10, where the

amplitude at the center of the aperture is plotted as a function of ka for $\phi_o = 10^o$ and $\phi_o = 30^o$. Not surprisingly the fields are larger for the larger aperture, but the general behavior is remarkably close to that found in ref. 1 for a circular aperture into a spherical cavity. The effect of oblique incidence is illustrated in Figures 11 and 12.

The program was also designed to compute the fields inside the cavity at sampled points along the line $\phi = 0$ from the center of the cavity to the aperture, and some data for the amplitudes as a function of position are presented in Figures 13 through 16. The curves are all for $\alpha = 0$, and the strong excitation when $\phi_o = 30$ and ka = 2.3 is very clear. Increasing α decreases the excitation, and this is shown in Figure 17 in which the amplitudes for $\alpha = 0(45^o)180^o$ and ka = 2.5 are plotted. To bring out the resonance effect, the field amplitude at the center of the cavity is plotted as a function of ka for $\phi_o = 10^o$ and $\phi_o = 30^o$ in Figure 18. As expected, opening up the aperture detunes the cavity and shifts its resonance to a lower frequency. This is more evident at the first resonance than at the second, and because of the sharpness of the first resonance, particularly for the smaller aperture, we have replotted the data of Figure 18 on a logarithmic scale in Figure 19.

In line with our original objective of investigating the integral equation approach in all phases of its operation, we have also given some attention to the complex frequency singularities of SEM. To locate a singularity, the program was run at each of a set of complex frequencies surrounding the expected value, with the program (in general) interrupted once the determinant had been computed. From an examination of the results, a new set of frequencies was selected, and so on until the zero of the determinant was found to the accuracy desired. No attempt was made to mechanize the procedure.

A plot of the first interior resonance as a function of the aperture half-angle ϕ_o is shown in Figure 20. Although any opening of the cavity must shift the frequency into the lower half of the complex ω plane and decrease its real part, the effect is very small for a 10^o angle, but increases rapidly with increasing ϕ_o. The computed values

are listed in Table 1, along with isolated data for other resonances. For the second

Table 1

SEM SINGULARITIES

$\omega c/a$ / ϕ_o, deg.	Interior		Exterior
	first	second	first
0	2.405	3.832	-2.404 - i 0.341
10	2.400 - i 0.001		
20	2.359 - i 0.015		
30	2.302 - i 0.067	3.827 - i 0.003	-2.38 - i 0.39
40	2.253 - i 0.160		

interior resonance, even $\phi_o = 30^o$ gives only a small shift in frequency comparable to that produced by $\phi_o = 10^o$ at the first resonance. The first exterior resonance proved more difficult to locate: the initial (sparse) sampling of the complex frequency plane pointed inexorably to the logarithmic singularity at $\omega = 0$, and only after a more detailed search was the zero found. As regards the determinants considered, it is believed that the data for the interior resonances given in Table 1 have at most an uncertainty of unity in the third decimal, but no statement of absolute accuracy is possible without a more detailed investigation of the effect that the number N of sampling points has.

SECTION IV
CONCLUSIONS

The results obtained leave little doubt that the E-field integral equation is an effective approach to the analysis of the thin-shell cavity problem, and provide encouragement for a study of a spherical cavity using the formulation given in ref. 2 .

However, the data for a circular cylinder are also of interest themselves, and it would seem desirable to pursue the present calculations further to locate more of the SEM singularities, including their complete dependence on ϕ_o, and their excitation coefficients.

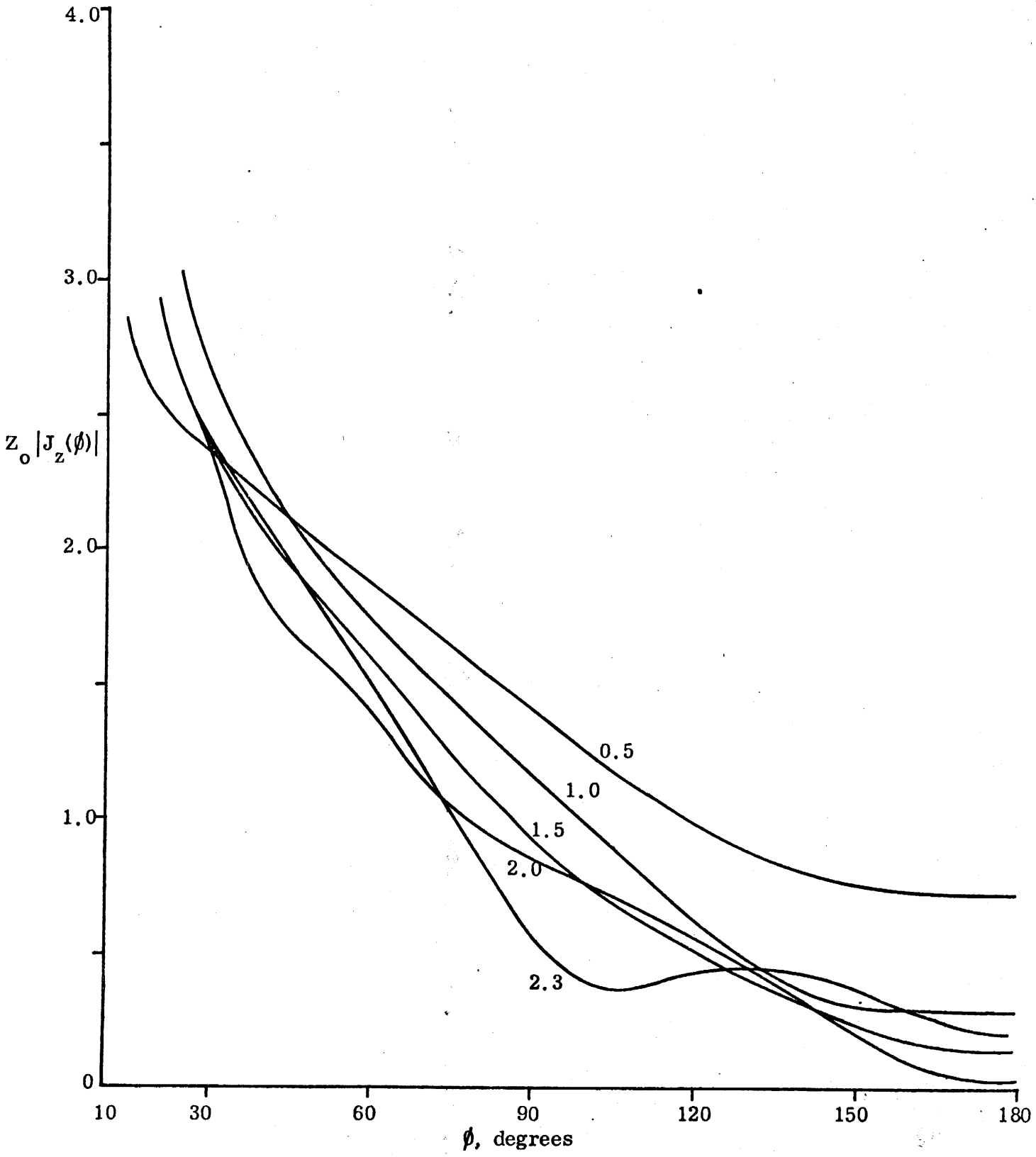

Figure 2. Shell current amplitudes for $\phi_o = 10^o$, $\alpha = 0$ and various values of ka.

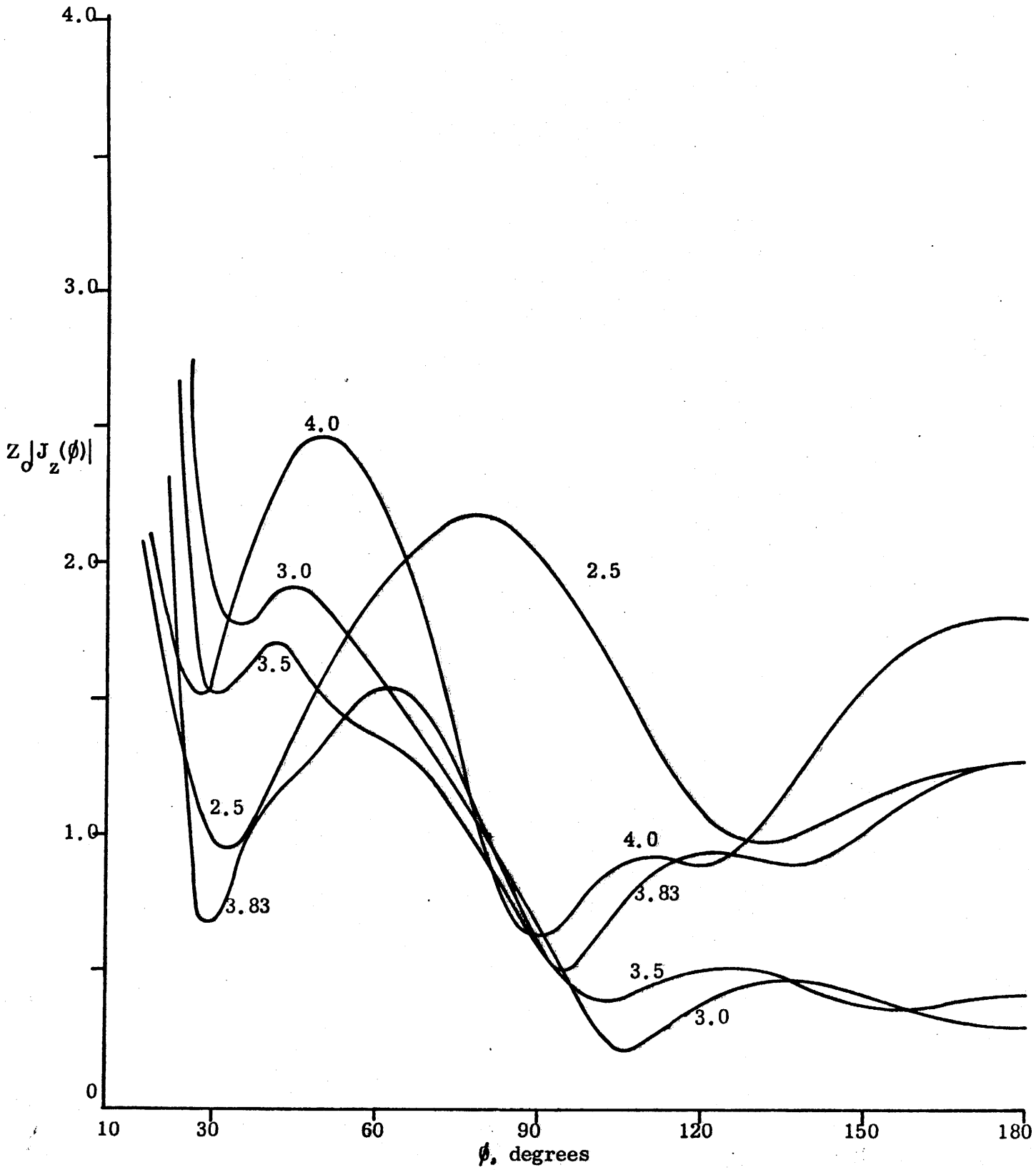

Figure 3. Shell current amplitudes for $\phi_o = 10^o$, $\alpha = 0$ and various values of ka.

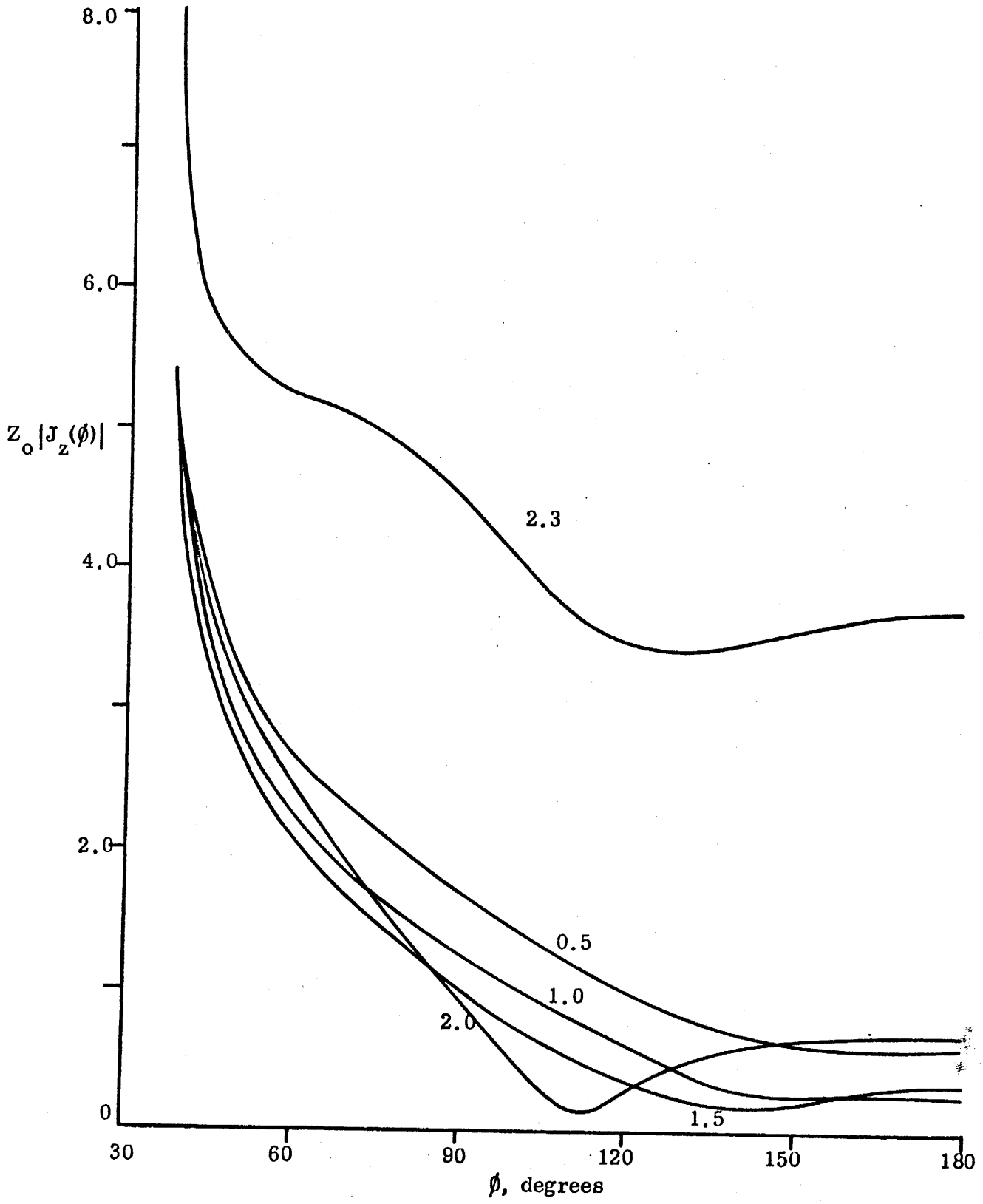

Figure 4. Shell current amplitudes for $\phi_o = 30^o$, $\alpha = 0$ and various values of ka.

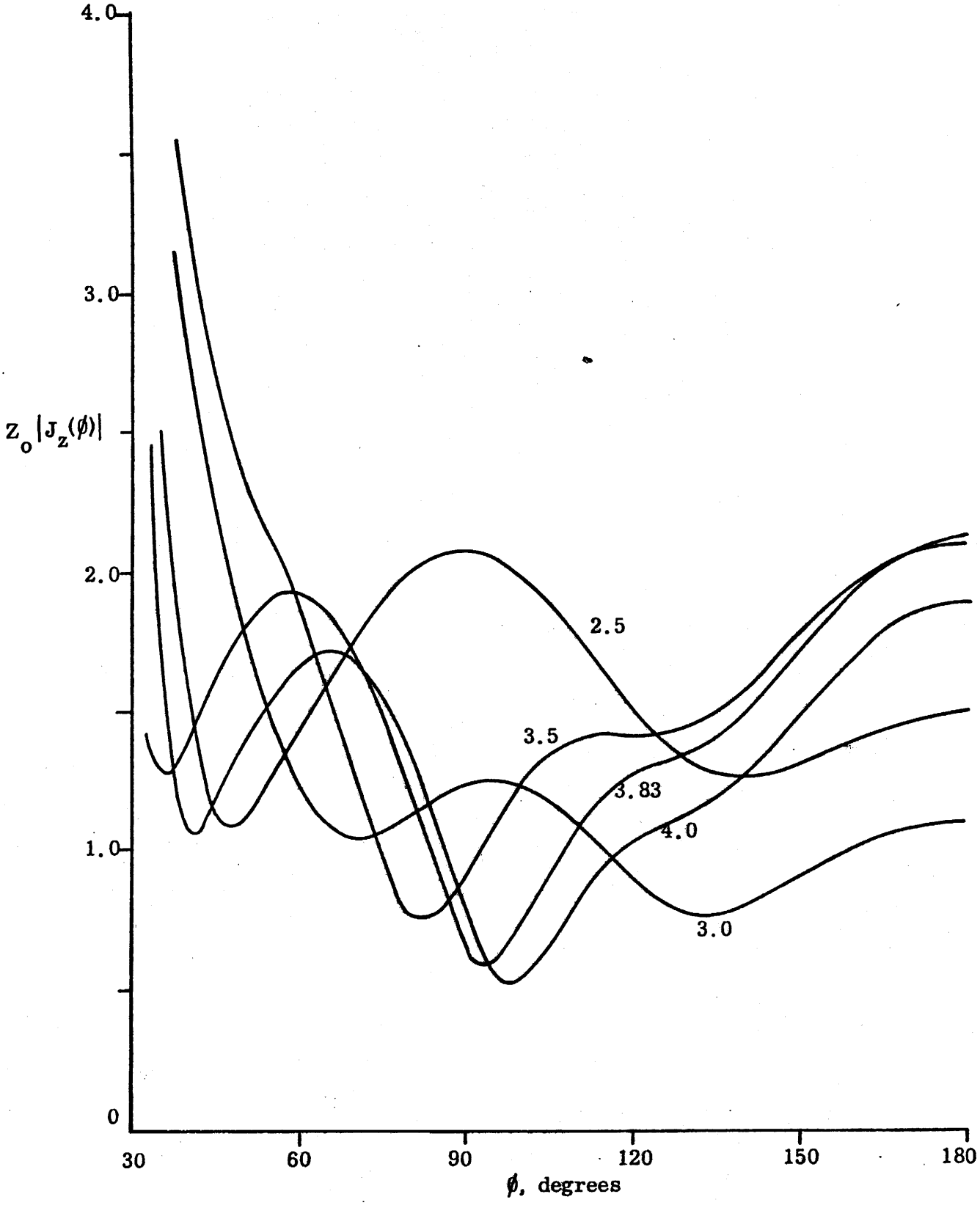

Figure 5. Shell current amplitudes for $\phi_o = 30^o$, $\alpha = 0$ and various values of ka.

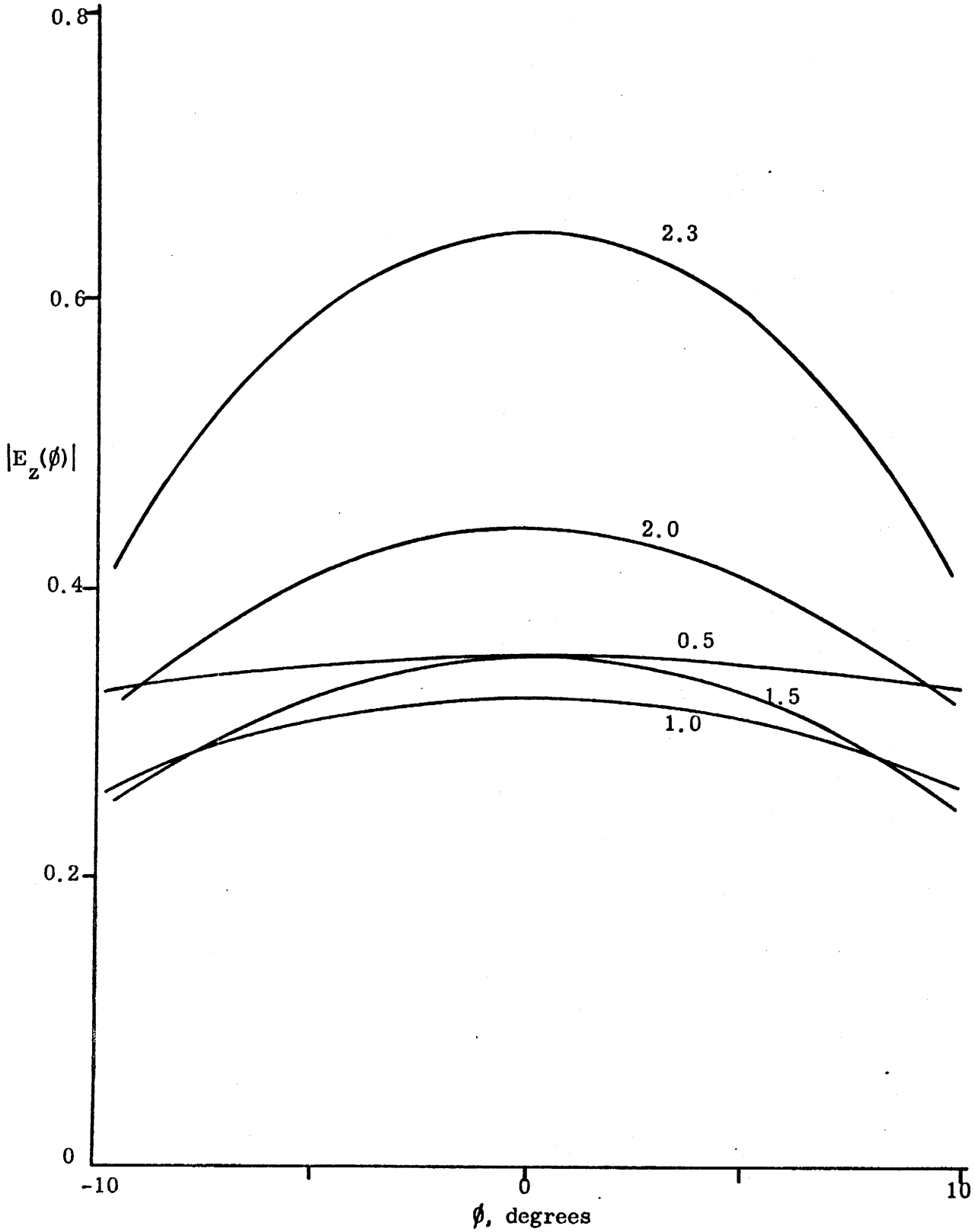

Figure 6. Aperture field amplitudes for $\phi_o = 10^o$, $\alpha = 0$ and various values of ka.

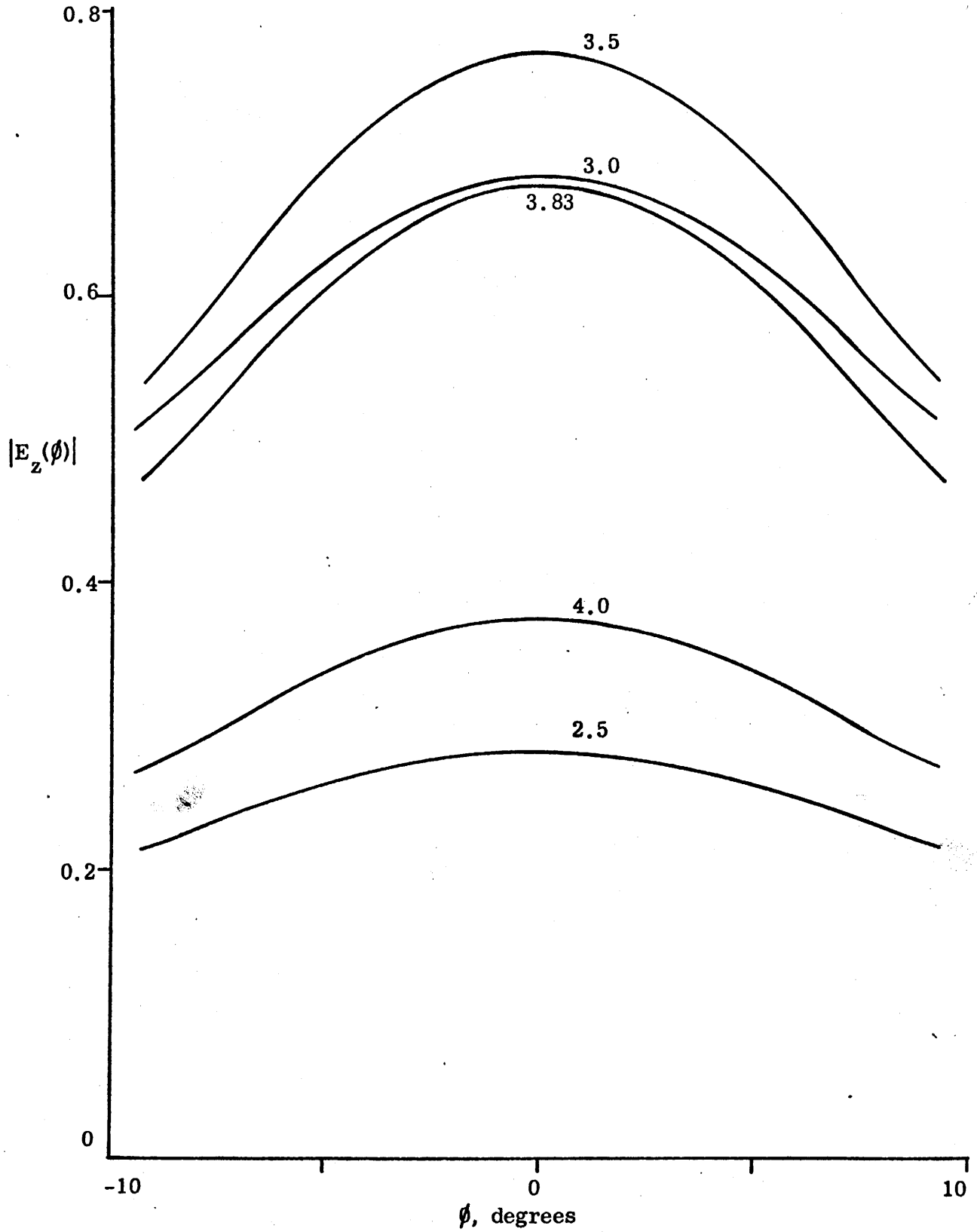

Figure 7. Aperture field amplitudes for $\phi_o = 10^o$, $\alpha = 0$ and various values of ka.

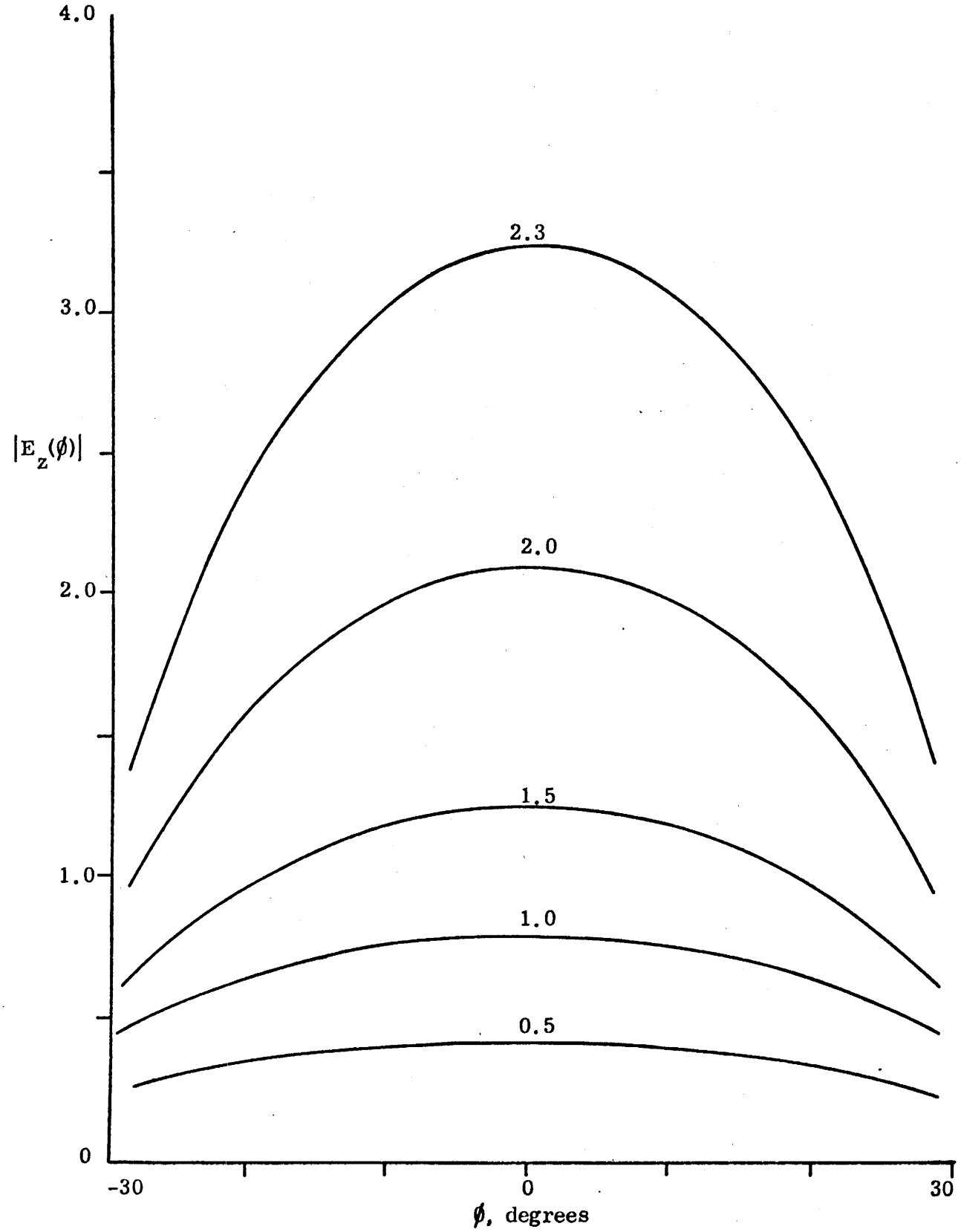

Figure 8. Aperture field amplitudes for $\phi_o = 30^o$, $\alpha = 0$ and various values of ka.

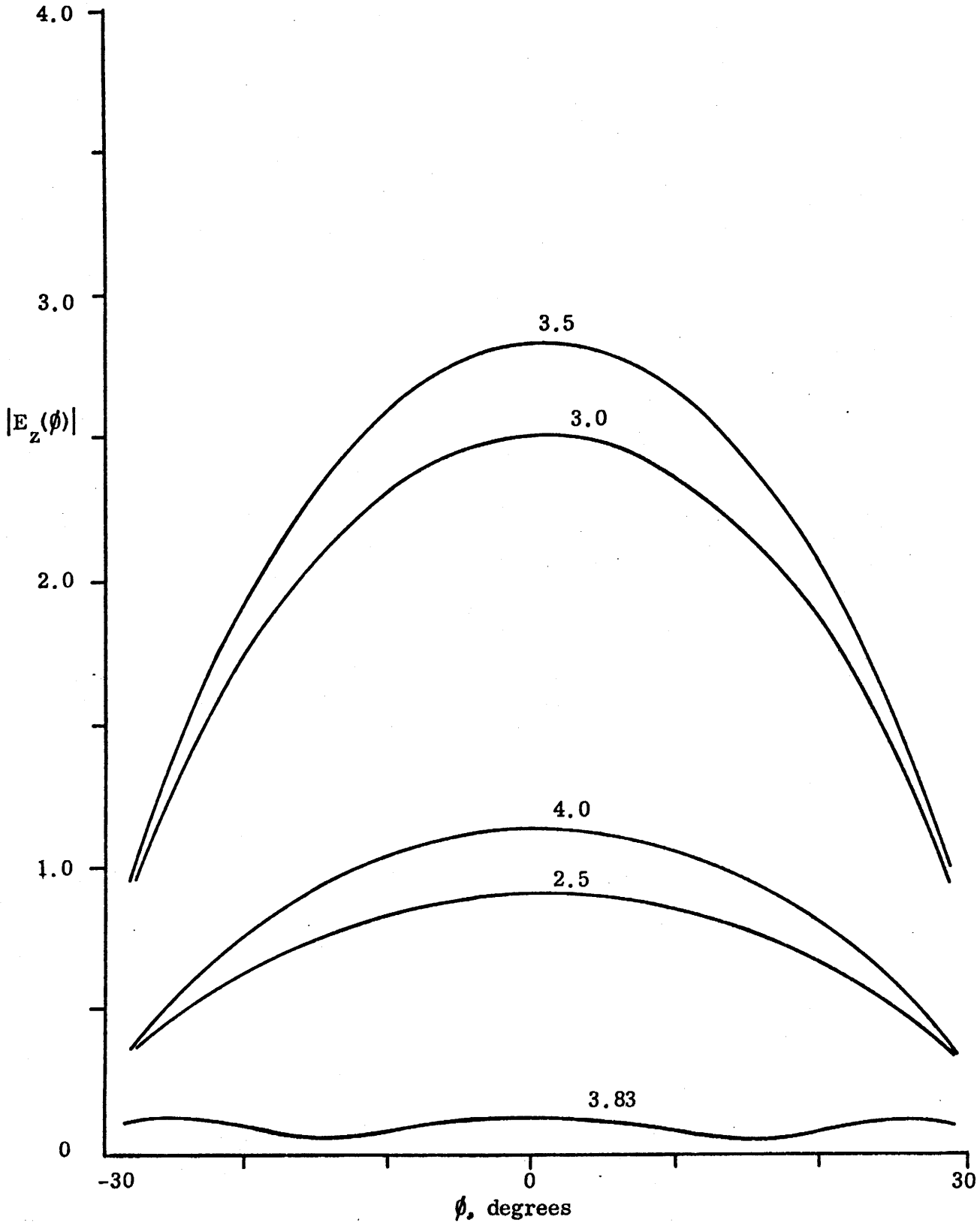

Figure 9. Aperture field amplitudes for $\phi_o = 30^o$, $\alpha = 0$ and various values of ka.

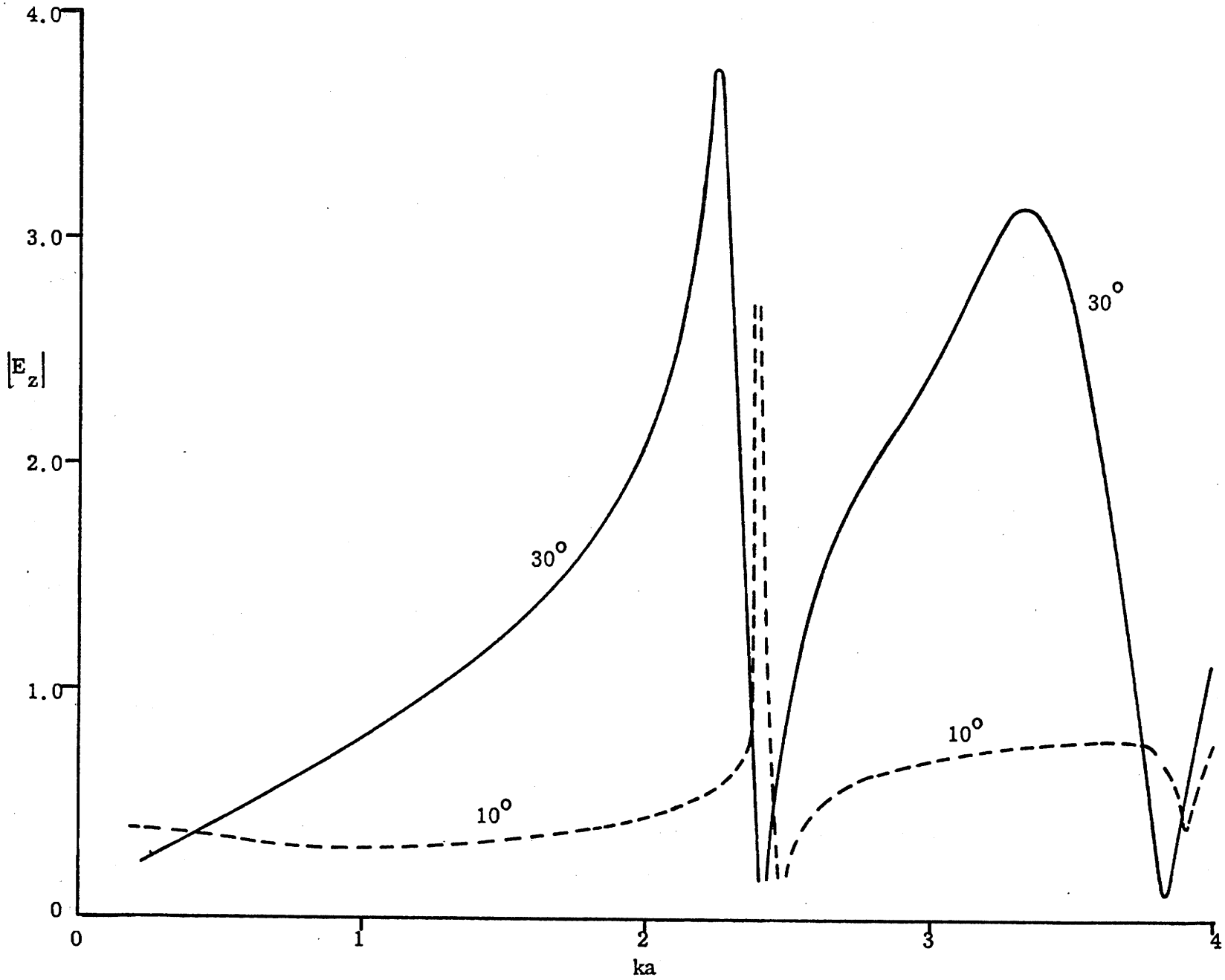

Figure 10. Field amplitude at the center of the aperture for $\phi_o = 10^o$ and 30^o, and $\alpha = 0$.

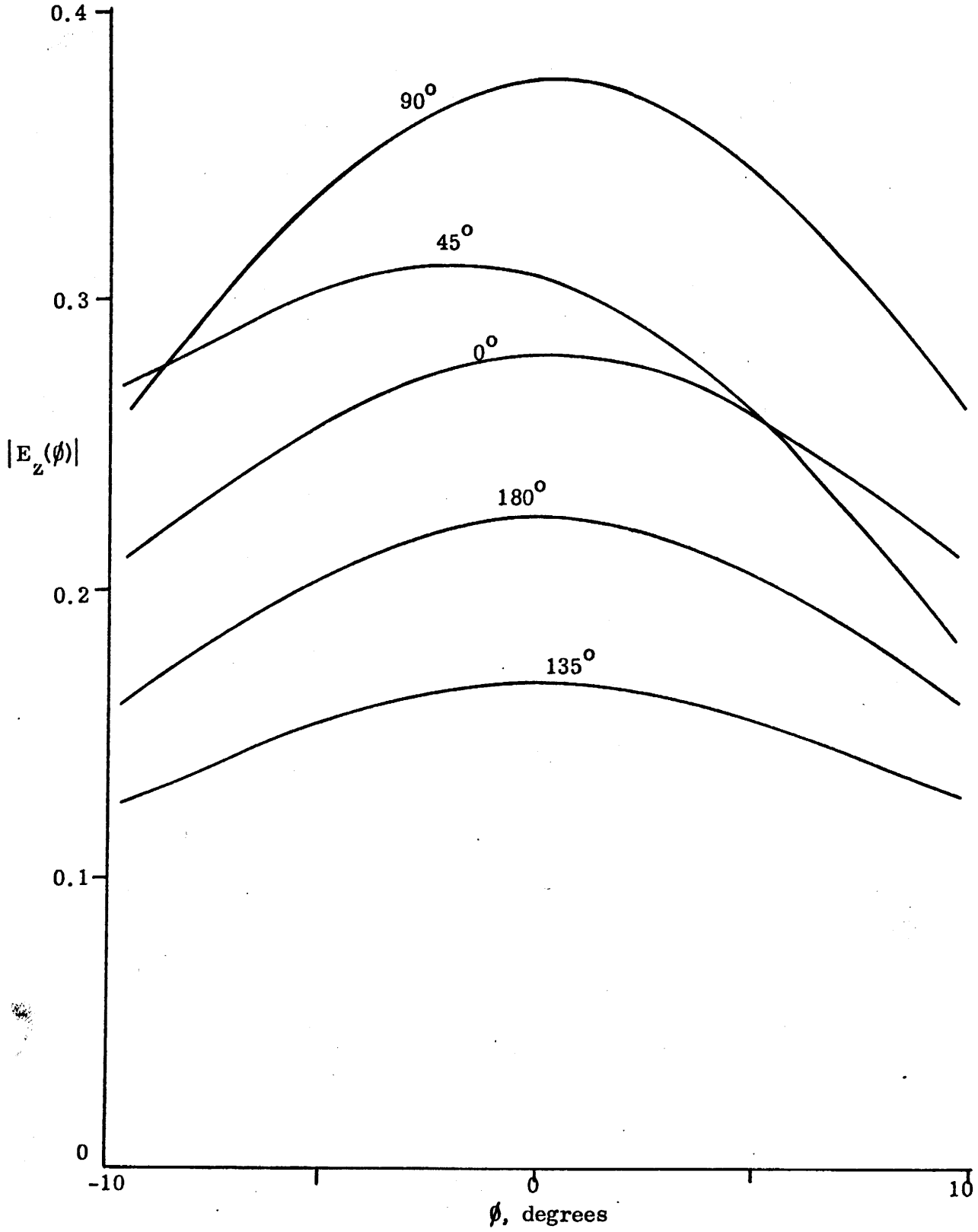

Figure 11. Aperture field amplitudes for $\phi_o = 10^o$, ka = 2.5 and $\alpha = 0(45^o)180^o$.

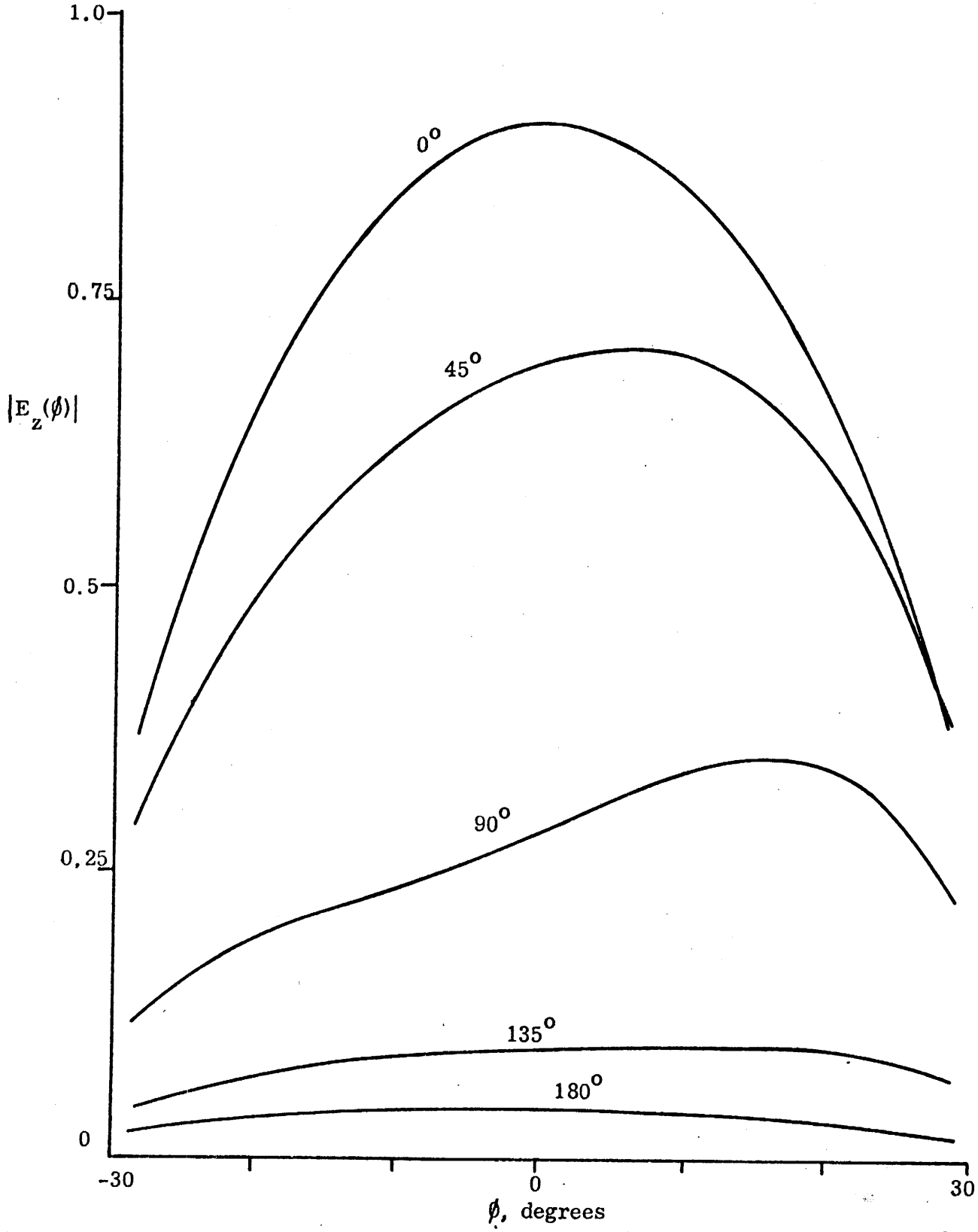

Figure 12. Aperture field amplitudes for $\phi_o = 30^o$, ka = 2.5 and $\alpha = 0(45^o)180^o$.

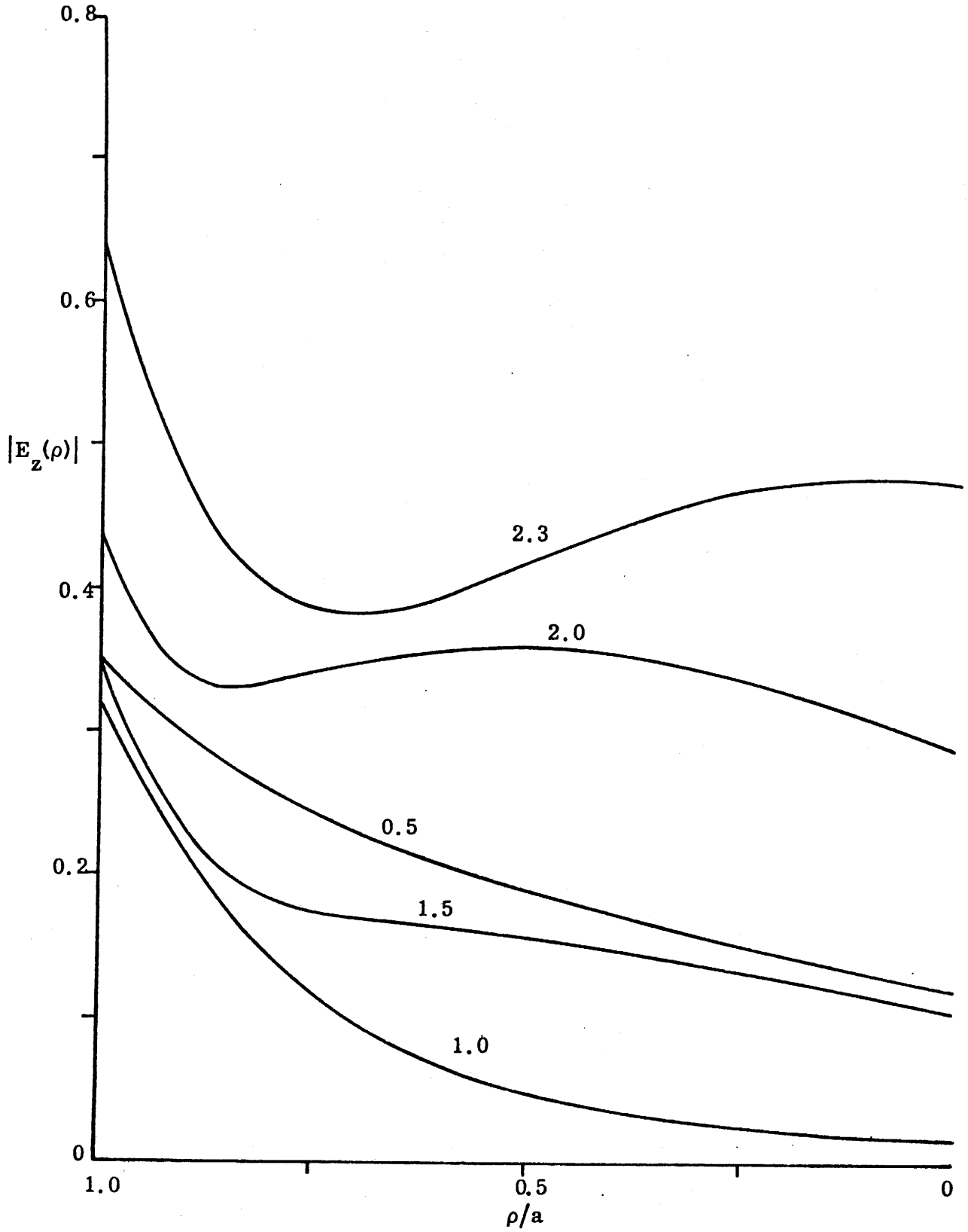

Figure 13. Interior field amplitudes for $\phi_o = 10^o$, $\alpha = 0$ and various values of ka.

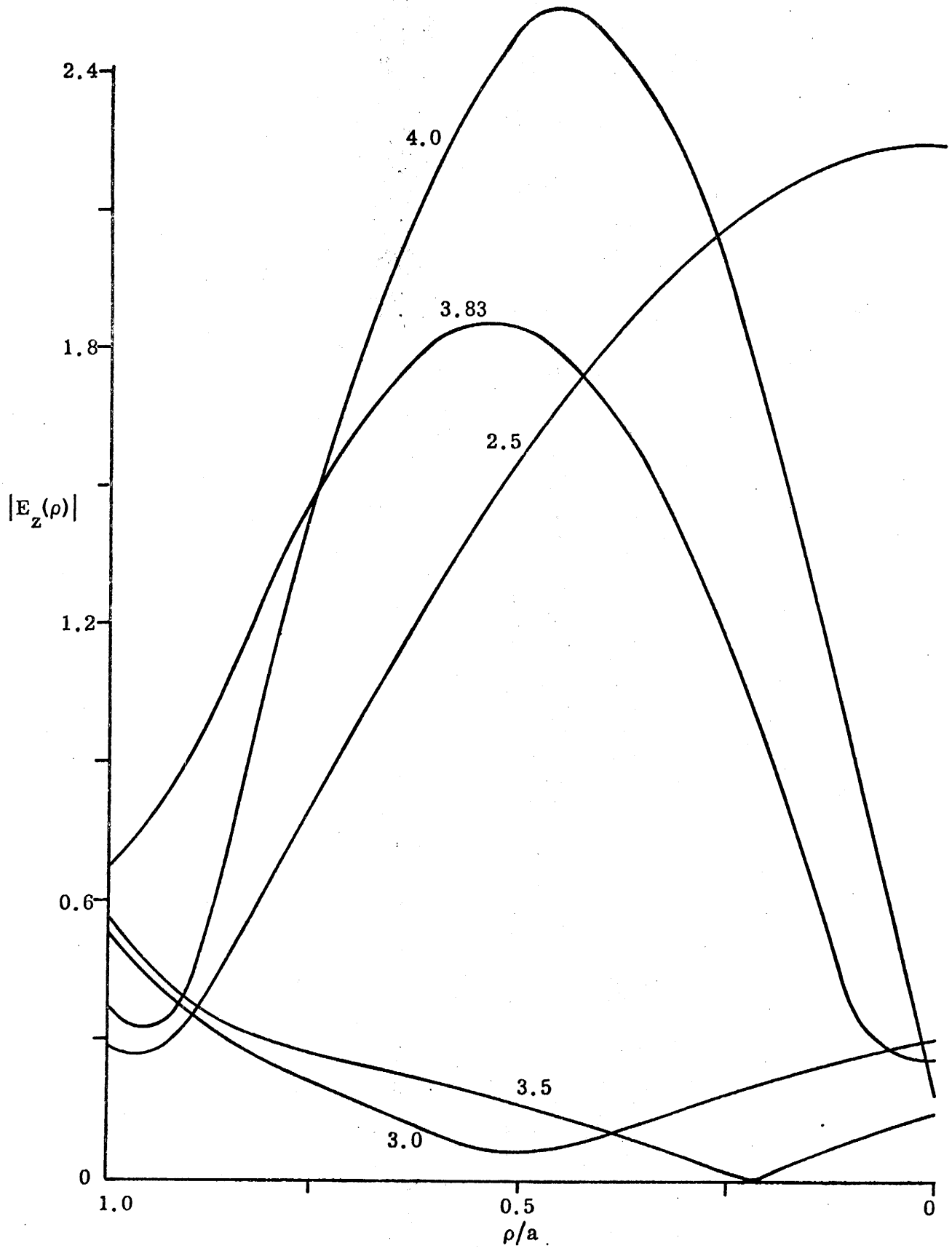

Figure 14: Interior field amplitudes for $\phi_o = 10^o$, $\alpha = 0$ and various values of ka.

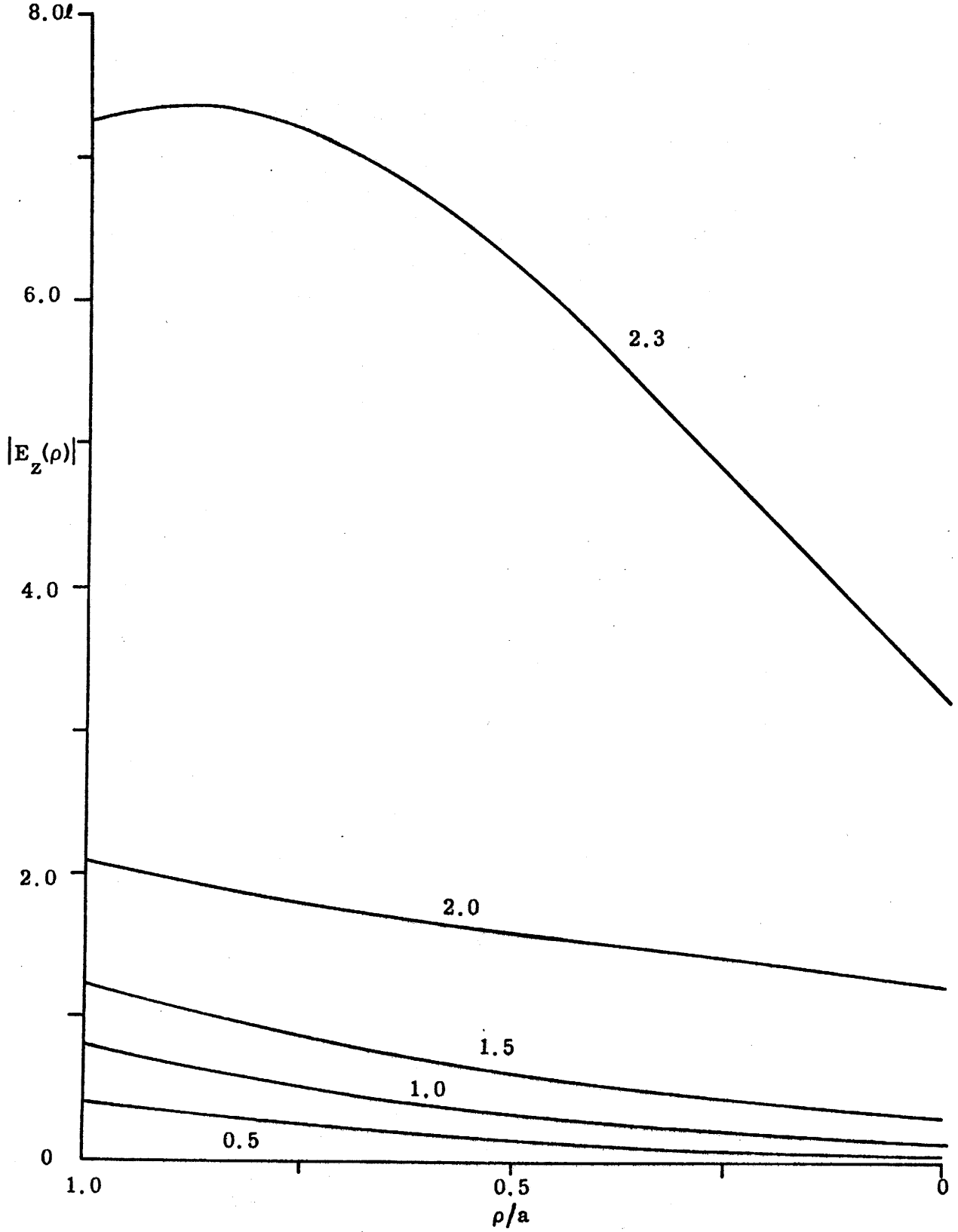

Figure 15. Interior field amplitudes for $\phi_o = 30^o$, $\alpha = 0$ and various values of ka.

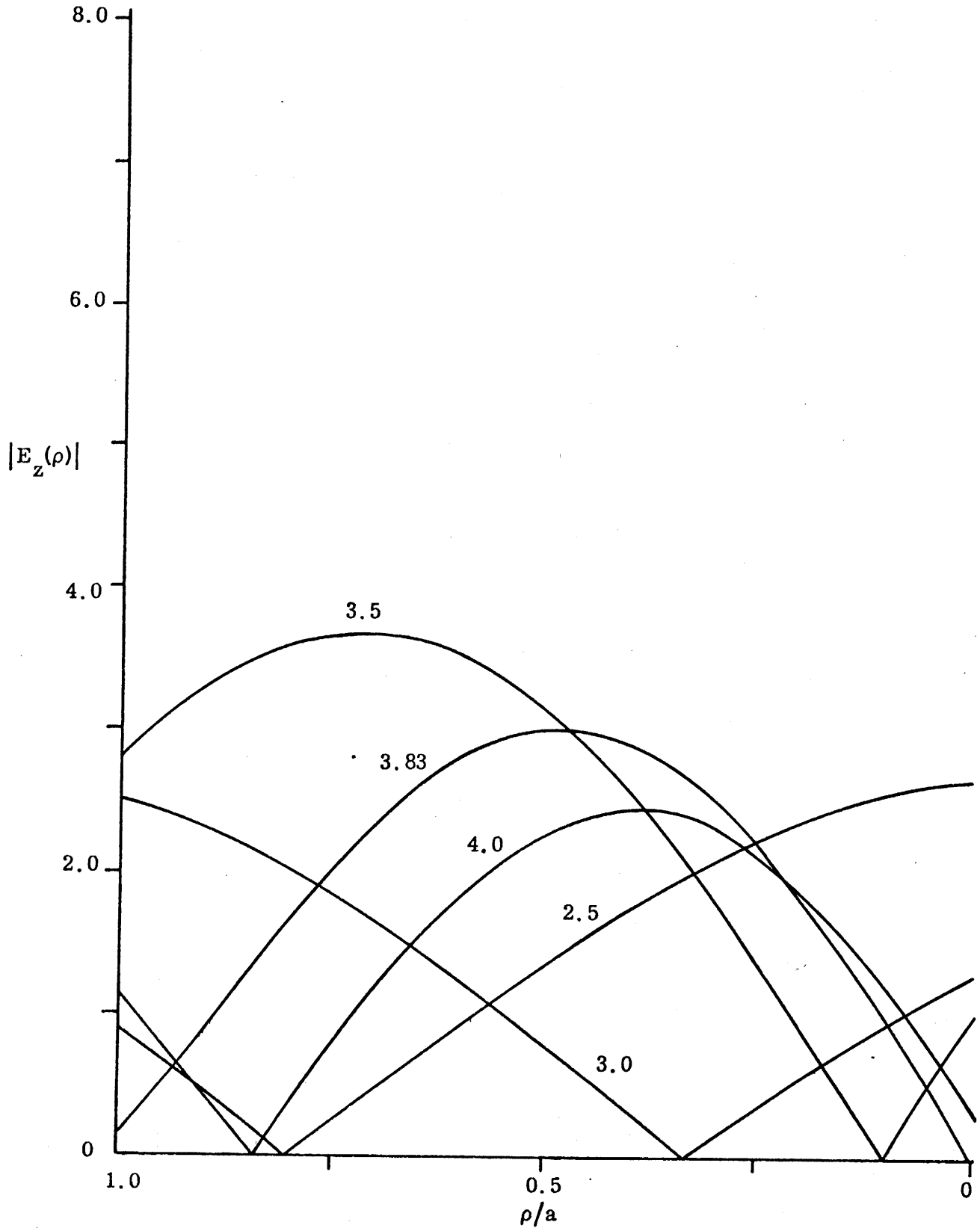

Figure 16. Interior field amplitudes for $\phi_o = 30^o$, $\alpha = 0$ and various values of ka.

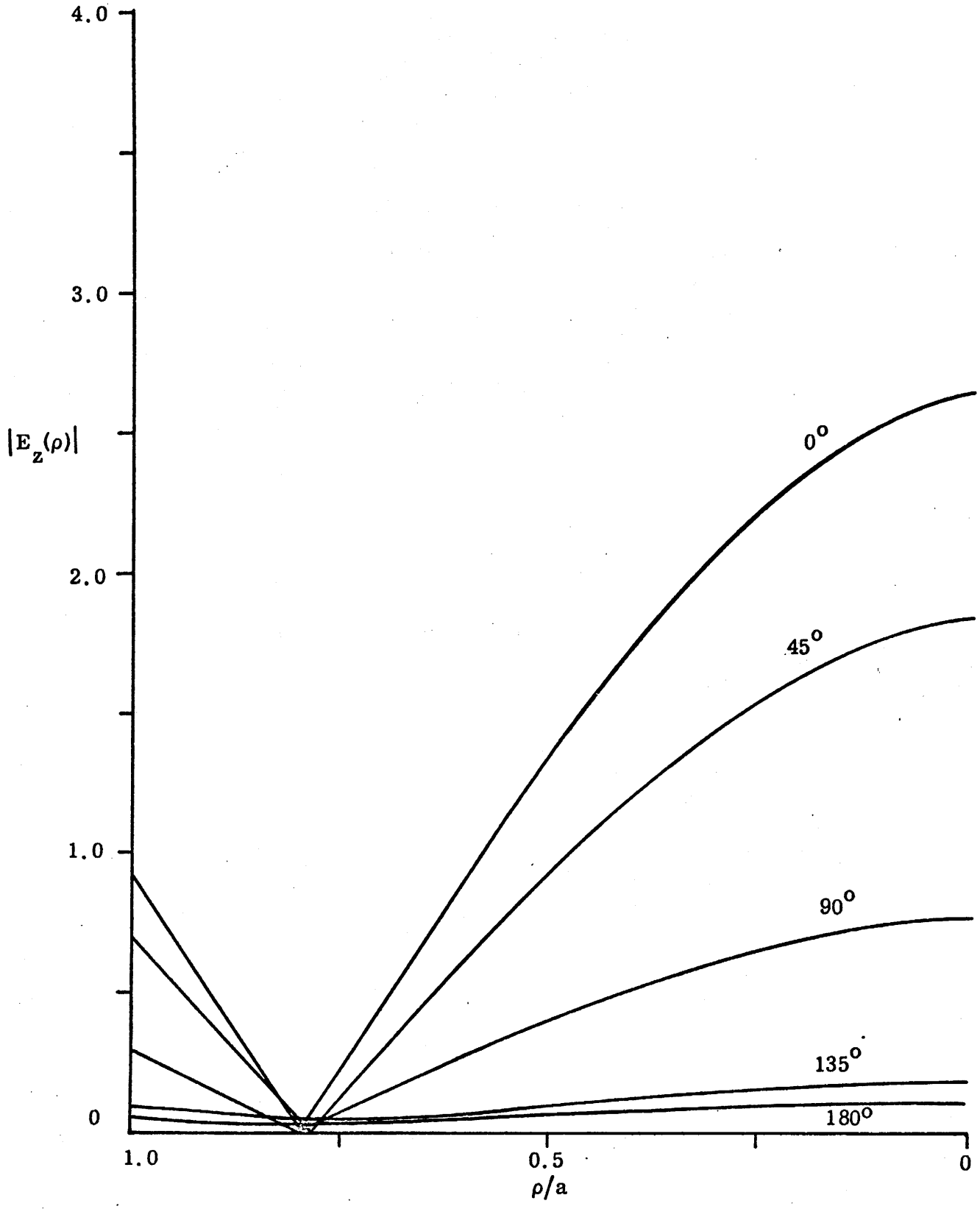

Figure 17. Interior field amplitudes for $\phi_o = 30^o$, ka = 2.5 and $\alpha = 0(45^o)180^o$.

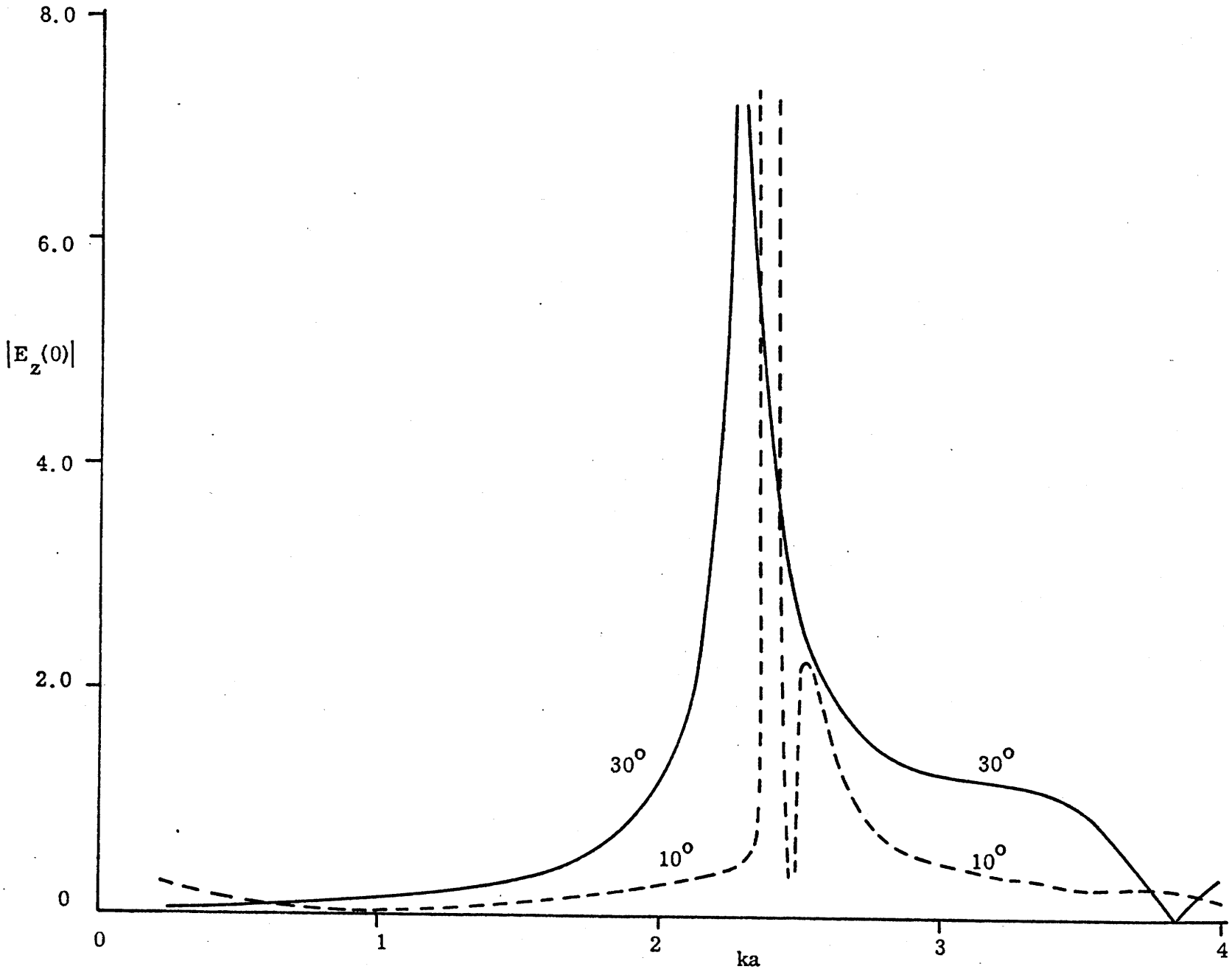

Figure 18. Field amplitude at the center of the cavity for $\phi_o = 10^o$ and 30^o, and $\alpha = 0$.

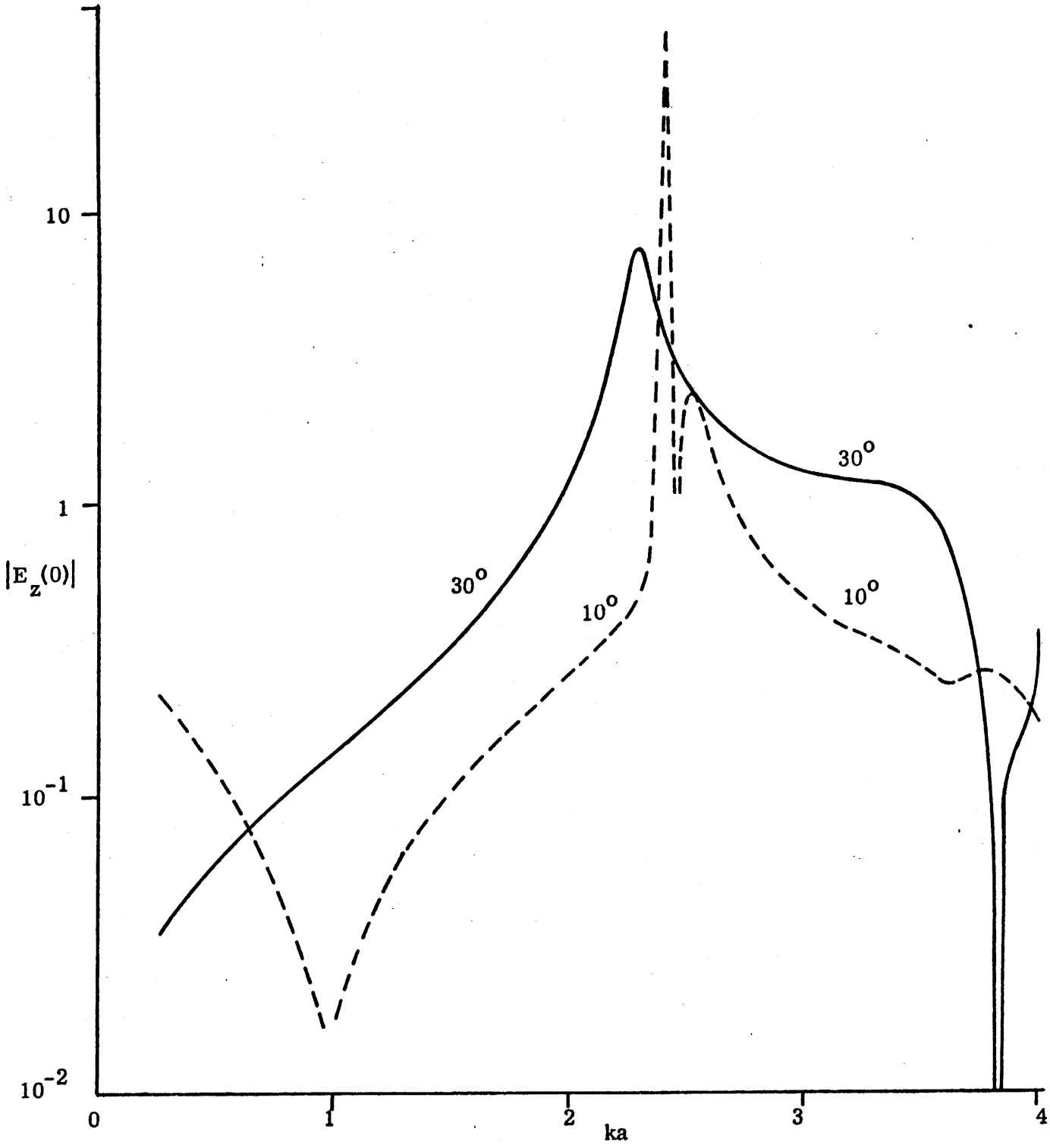

Figure 19. Field amplitude at the center of the cavity for $\phi_o = 10^o$ and 30^o, and $\alpha = 0$.

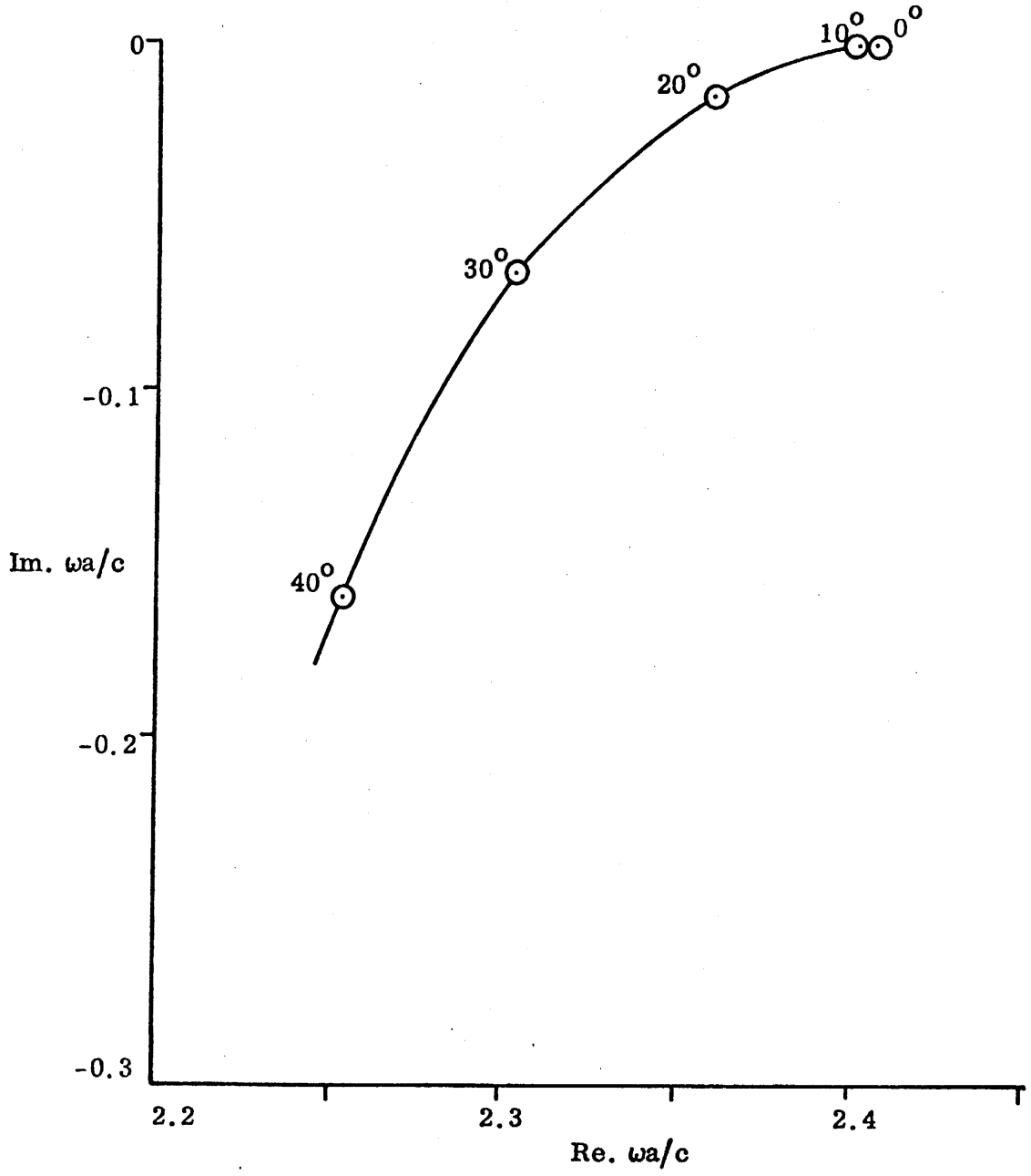

Figure 20. First interior resonance for $0 \leq \phi_o \leq 40^o$.

REFERENCES

1. T.B.A. Senior and G.A. Desjardins, Field Penetration into a Spherical Cavity, Interaction Note No. 142, August 1973. See also IEEE Trans. EMC-16, 205-208, 1974.

2. T.B.A. Senior, The Spherical Cavity Problem, Interaction Note No. 220, January 1975.

3. E.F. Knott, V.V. Liepa and T.B.A. Senior, Non-Specular Radar Cross Section Study, 011062-1-F (AFAL-TR-73-70), The University of Michigan Radiation Laboratory, Ann Arbor, Michigan, 1973.

4. V.V. Liepa, E.F. Knott and T.B.A. Senior, Scattering from Two-Dimensional Bodies with Absorber Sheets, 011764-2-T, The University of Michigan Radiation Laboratory, Ann Arbor, Michigan, 1974.

5. M. Abramowitz and I.A. Stegun, Handbook of Mathematical Functions, National Bureau of Standards Applied Math. Series 55, U.S. Department of Commerce, 1964, pp. 359, 373.

6. E. Jahnke and E. Emde, Tables of Functions, Dover Pub., New York, 1945.

APPENDIX

SLOTTED CYLINDER COMPUTER PROGRAM

INTRODUCTION

We here describe the essential features of the computer program that solves the two-dimensional integral equation (3) for the total current induced in the wall of a perfectly conducting cylindrical shell having a longitudinal slot. The electrical size of the cylinder and the angular size of the slot are the only body variables subject to control by the user of the program, but there is no limit to the number of angles of incidence that may be specified.

The program is named RAMP and is written in FORTRAN for MTS (Michigan Terminal Service) at the University of Michigan, where the basic machine is an IBM 360 computer. Because some features of the MTS system differ from those of other computer facilities, minor alterations would have to be made if RAMP were run elsewhere. The program is patterned after others developed at the Radiation Laboratory that solve similar two-dimensional problems but involving more general profiles. However, little attempt has been made to exploit the specific symmetry of the slotted circular cylinder, so that the program is not as efficient as it might be. The matrix for this geometry is, for example, symmetric, and the running time could be reduced somewhat were this symmetry to be used.

MATHEMATICAL FORMULATION

The program solves the E field integral equation (3) for any complex number k whose real part is the free space propagation constant. The contour C extends from one edge of the slot to the other along the cylindrical shell, and is subdivided into M cells, where M is an integer specified on input. Thus, each cell has an angular width

$$\Delta \phi = 2(\pi - \phi_o)/M$$

where ϕ_o is the half angle subtended by the slot. The width chosen reflects the judgement of the user, since small widths tend to improve accuracy but also to increase machine running time. Much recent data generated by RAMP were obtained using cell widths of $\lambda/12$ or less, implying

$$M \geq 12\ ka.$$

The linearlization of eq. (3) produces M simultaneous equations for the unknown currents J_z, assumed constant over each cell. Program RAMP creates an M x M matrix of complex numbers associated with this system of equations, inverts the matrix and then multiplies the resultant matrix by the incident field to obtain the surface currents. The currents, now being known, may be used to calculate the scattered electric field at any point in space from eq. (2). In the actual computation, of course, the program approximates the integral by a discrete sum of M contributions.

Although eq. (2) allows the fields to be calculated anywhere, the program is very specific and computes them only over the slot aperture (at constant radius a) and along a radius that terminates at the midpoint of the slot. Moreover, it is the total field that is computed, so that once the integration required by eq. (2) is performed, the program then adds the incident field (1) to obtain the total field.

PROGRAM DESCRIPTION

Program RAMP is an outgrowth of a previous, more efficient version in which the wavenumber k was a pure real number. In general, however, the interior resonances occur at complex wavenumbers, especially for aperture half angles greater than about 10 degrees, hence the generalization to complex k was necessary. In order to achieve this, two modifications were made: a) the provision of a complex number (KFAC in the program) which is chosen by the user, specified on input and subsequently multiplied by the (real) free space wavenumber to generate complex k, and b) the development of a subroutine to generate Hankel functions for complex arguments. It is mainly this latter provision that makes RAMP less efficient than its predecessor.

RAMP consists of a MAIN program and two subroutines, FLIP and HANK, MAIN reads all input, prints all output, fills the matrix elements, computes the field distributions from the current distribution and indexes through the desired range of incidence angles. FLIP performs two functions; it inverts the original matrix and multiplies the inverted matrix by the incident field to obtain the surface currents. The bulk of FLIP is virtually a copy of IBM's matrix inversion routine, but modified for complex elements, with a handful of statements added at the end to perform the matrix multiplication operation. The MAIN program prudently calls for the inversion from FLIP only once, and thereafter expects FLIP to merely supply new current distributions for new angles of incidence.

Subroutine HANK is based on the ascending series representation for the Bessel functions of the first and second kinds of order zero. The program decides how many terms of the series to use from the criterion

$$n = 6 + 1.35\,|W| \ ,$$

where n is the number of terms used and W is the complex argument. Although the criterion was selected so as to provide absolute precision of better than 10^{-5}, internal round-off errors tend to be worse than this for complex arguments having large imaginary parts. For real W the accuracy is better than 10^{-5} for arguments as large as 10.0. Since HANK uses double precision arithmic on the IBM 360, it would have to be modified for, say, the CDC-6600 system.

Briefly, the program RAMP operates as follows: input data for a single frequency and aperture half angle are read from two consecutive cards from the input stream, as described below. The first entry on the first card is the integer M (the number of sampling points on the cylinder profile) and is also used as a key to shut down the program; i.e., if M = 0 — which can be synthesized with a blank card — the program terminates. The MAIN program then fills the matrix, calling on subroutine HANK for

the appropriate Hankel functions. The incident field structure is computed for the first angle of incidence and MAIN then calls FLIP to invert the matrix and supply the current at each cell on the profile.

The currents are weighted and summed according to eq. (2) to obtain the total electric field distribution at N discrete points over the aperture and at L discrete points along a radius. N and L are controlled by the user as input data. Since the weighting function is a Hankel function, much of the machine time is spent carrying out operations in subroutine HANK. After the fields over the aperture and along a radius have been computed and printed on the output record, MAIN indexes to the next angle of incidence by adding an increment (specified as input data). Subroutine FLIP is called, but since the matrix has already been inverted, FLIP merely supplies new values for the surface currents, which MAIN then uses to compute new field distributions. If the new angle of incidence exceeds the limit specified by the user, the program returns to the input stream and reads the first of a pair of cards required to specify a new geometry. As mentioned earlier, a blank card will shut down the program.

INPUT DATA FORMAT

The two input data cards required for a single geometry should contain the following information:

Card 1: FORMAT (315)

M the number of sampling points on the profile,

N the number of field points in the aperture,

L the number of field points along the radius.

Card 2; FORMAT (8F10. 5)

A the radius of the cylinder in inches,

HANG the aperture half-angle in degrees,

WAVE the incident wavelength in inches,

KFAC a complex number whose real part (always 1. 0) and imaginary part constitute the fourth and fifth entries on the card,

FIRST the first angle of incidence in degrees,

LAST the last angle of incidence in degrees,

INK the increment to be used in indexing through the incidence angles.

In hindsight, the variables A, WAVE and KFAC could have been incorporated in a single complex variable (say KA) making the input structure a little less complicated, but at the time the program was being prepared the variations to be studied were not known precisely. This is because the previous version of RAMP (for real ka only) was modified by the inclusion of the factor KFAC to permit complex values for ka. Consequently the user must decide beforehand what value of (complex) ka is of interest, then calculate A, WAVE and KFAC to be read in as input in order to generate this value.

PROGRAM LISTING

A listing of the main program and the two subroutines are given on pages 36 through 39. The entire program occupies 30584 32-bit bytes of storage as listed; the required storage will change, of course, if the arrays are re-dimensioned so as to accommodate other cylinders (i.e., different surface field sampling points). The program is presently limited to 50 sampling points.

OUTPUT SAMPLE

Pages 40 and 41 contain a sample of output to illustrate the format. The first page lists the current distribution over the cylinder surface and the second lists the total field distributions over the aperture and along a radius.

```
      IMPLICIT COMPLEX(K)
      COMPLEX AA(50,51),KJ(50),PINK(50),SUM,B
      REAL LAST,INK
      DIMENSION FEE(50),FEAT(50)
      DATA RED,DIG/0.01745329,57.29578/
10    READ 100, M,N,L
      IF (M.EQ.0) GO TO 95
      READ 200, A,HANG,WAVE,KFAC,FIRST,LAST,INK
      K=6.283185*KFAC/WAVE
      KA=K*A
      KTA=2.0*KA
      DEEFEE=2.0*(180.0-HANG)/M
      DEFEAT=RED*DEEFEE
      ADFEE=A*DEFEAT/WAVE
      KDA=0.25*KA*DEFEAT
      DO 15 I=1,M
      FEE(I)=HANG+DEEFEE*(I-0.5)
15    FEAT(I)=RED*FEE(I)
      DO 35 I=1,M
      DO 35 J=1,M
      IF (I.EQ.J) GO TO 25
      ANG=ABS(FEAT(I)-FEAT(J))*0.5
      SANG=SIN(ANG)
      KR=KTA*SANG
      CALL HANK(KR,KH)
      AA(I,J)=KDA*KH
      GO TO 35
25    AA(I,J)=ADFEE*CMPLX(1.570796,0.02879837+ALOG(ADFEE))
35    CONTINUE
      DEL=2.0*HANG/N
      TETA=FIRST-INK
40    TETA=TETA+INK
      IF (TETA.GT.LAST) GO TO 10
      THE=RED*TETA
      DO 45 I=1,M
      KANG=KA*COS(THE-FEAT(I))*CMPLX(0.0,-1.0)
45    PINK(I)=CEXP(KANG)
      IF (TETA.EQ.FIRST) GO TO 50
      CALL FLIP(AA,M,PINK,KJ,SUM,ANG,2)
      GO TO 62
50    CALL FLIP(AA,M,PINK,KJ,B,DMAG,1)
55    PRINT 400, KA,HANG,TETA,DMAG
      PRINT 300
      DO 60 I=1,M
      AMP=CABS(KJ(I))
      FASE=DIG*ATAN2(AIMAG(KJ(I)),REAL(KJ(I)))
60    PRINT 500, I,FEE(I),AMP,FASE,I
62    PRINT 700, KA,HANG,TETA
      PRINT 900
      DO 75 J=1,N
      SUM=CMPLX(0.0,0.0)
      ANGLE=DEL*(J-0.5)-HANG
      ANG=RED*ANGLE
      DO 70 I=1,M
      SANG=SIN(0.5*ABS(ANG-FEAT(I)))
```

```
      KR=KTA*SANG
      CALL HANK(KR,KH)
   70 SUM=SUM-KJ(I)*KH
      SUM=KDA*SUM
      KANG=KA*COS(THE-ANG)*CMPLX(0.0,-1.0)
      SUM=SUM+CEXP(KANG)
      AMP=CABS(SUM)
      FASE=DIG*ATAN2(AIMAG(SUM),REAL(SUM))
   75 PRINT 600, ANGLE,SUM,AMP,FASE
      IF (L+N.LT.47) GO TO 82
      PRINT 700, KA,HANG,TETA
   82 PRINT 800
      DIP=A/L
      LL=L+1
      DO 90 J=1,LL
      R=DIP*(J-1)
      RA=R/A
      SUM=CMPLX(0.0,0.0)
      DO 85 I=1,M
      KR=KA*SQRT(1.0+RA*(RA-2.0*COS(FEAT(I))))
      CALL HANK(KR,KH)
   85 SUM=SUM-KJ(I)*KH
      SUM=KDA*SUM
      KANG=K*R*COS(THE)*CMPLX(0.0,-1.0)
      SUM=SUM+CEXP(KANG)
      AMP=CABS(SUM)
      FASE=DIG*ATAN2(AIMAG(SUM),REAL(SUM))
   90 PRINT 600, R,SUM,AMP,FASE
      GO TO 40
   95 CALL SYSTEM
  100 FORMAT (3I5)
  200 FORMAT (8F10.5)
  300 FORMAT (' CELL NUMBER    ANGLE     CURRENT AMPLITUDE  ',
     &'CURRENT PHASE   CELL NUMBER'/)
  400 FORMAT ('1',27X,'SLOTTED CYLINDER'/20X,'KA',14X,2F8.3/20X,
     &'APERTURE HALF-ANGLE',F13.3/20X,'INCIDENT FIELD DIRECTION',
     &F8.3/20X,'DETERMINANT',E21.5//)
  500 FORMAT (I7,F15.2,F17.5,F16.2,I12)
  600 FORMAT (F9.2,F17.5,F12.5,F16.5,F14.2)
  700 FORMAT ('1',27X,'SLOTTED CYLINDER'/20X,'KA',14X,2F8.3/20X,
     &'APERTURE HALF-ANGLE',F13.3/20X,'INCIDENT FIELD DIRECTION',F8.3/)
  800 FORMAT ('0 DISTANCE',8X,'FIELDS ALONG A RADIUS',7X,'AMPLITUDE',
     &8X,'PHASE'/)
  900 FORMAT ('0   ANGLE',12X,'APERTURE FIELDS',10X,'AMPLITUDE',
     &8X,'PHASE'/)
      END
```

```
      SUBROUTINE FLIP(A,N,X,Y,D,DMAG,IAT)
      COMPLEX A(50,51),X(50),Y(50),D,BIGA,HOLD
      DIMENSION L(50),M(50)
      IF (IAT.GT.1) GO TO 150
      D=CMPLX(1.0,0.0)
      DO 80 K=1,N
      L(K)=K
      M(K)=K
      BIGA=A(K,K)
      DO 20 J=K,N
      DO 20 I=K,N
   10 IF (CABS(BIGA).GE.CABS(A(I,J))) GO TO 20
      BIGA=A(I,J)
      L(K)=I
      M(K)=J
   20 CONTINUE
      J=L(K)
      IF (J.LE.K) GO TO 35
      DO 30 I=1,N
      HOLD=-A(K,I)
      A(K,I)=A(J,I)
   30 A(J,I)=HOLD
   35 I=M(K)
      IF (I.LE.K) GO TO 45
      DO 40 J=1,N
      HOLD=-A(J,K)
      A(J,K)=A(J,I)
   40 A(J,I)=HOLD
   45 IF (CABS(BIGA).NE.0.0) GO TO 50
      D=CMPLX(0.0,0.0)
      RETURN
   50 DO 55 I=1,N
      IF (I.EQ.K) GO TO 55
      A(I,K)=-A(I,K)/BIGA
   55 CONTINUE
      DO 65 I=1,N
      DO 65 J=1,N
      IF (I.EQ.K.OR.J.EQ.K) GO TO 65
      A(I,J)=A(I,K)*A(K,J)+A(I,J)
   65 CONTINUE
      DO 75 J=1,N
      IF (J.EQ.K) GO TO 75
      A(K,J)=A(K,J)/BIGA
   75 CONTINUE
      D=D*BIGA
   80 A(K,K)=1.0/BIGA
      BN=FLOAT(N)
      DMAG=CABS(D)*(2.0**BN)
      K=N
  100 K=K-1
      IF (K.LE.0) GO TO 150
      I=L(K)
      IF (I.LE.K) GO TO 120
      DO 110 J=1,N
      HOLD=A(J,K)
```

```
      A(J,K)=-A(J,I)
110   A(J,I)=HOLD
120   J=M(K)
      IF (J.LE.K) GO TO 100
      DO 130 I=1,N
      HOLD=A(K,I)
      A(K,I)=-A(J,I)
130   A(J,I)=HOLD
      GO TO 100
150   DO 200 I=1,N
      Y(I)=CMPLX(0.0,0.0)
      DO 200 J=1,N
200   Y(I)=A(I,J)*X(J)+Y(I)
      RETURN
      END



      SUBROUTINE HANK(Z,H)
      COMPLEX Z,H
      COMPLEX*16 J,Y,ZZ,DUM
      REAL*8 A,B,F
      A=DBLE(REAL(Z))
      B=DBLE(AIMAG(Z))
      ZZ=-0.25*DCMPLX(A*A-B*B,2.0*A*B)
      F=CDABS(ZZ)
      X=SNGL(F)
      MM=6+IFIX(1.35*X)
      F=1.0
      MM=MM-1
      DO 10 K=2,MM
      B=1.0/DFLOAT(K)
10    F=F+B
      B=1.0/DFLOAT(K+1)
      A=DFLOAT(K*K)
      DUM=ZZ/A
      J=1.0+DUM
      Y=F+(F+B)*DUM
      DO 30 I=1,MM
      K=MM-I+1
      B=1.0/DFLOAT(K)
      A=DFLOAT(K*K)
      DUM=ZZ/A
      F=F-B
      Y=F+DUM*Y
30    J=1.0+DUM*J
      Y=(0.57721566490153+CLOG(0.5*Z))*J-Y
      Y=0.6366198*Y
      A=DREAL(J)-DIMAG(Y)
      B=DIMAG(J)+DREAL(Y)
      H=CMPLX(SNGL(A),SNGL(B))
      RETURN
      END
```

SLOTTED CYLINDER

KA 2.300 -0.200

APERTURE HALF-ANGLE 30.000

INCIDENT FIELD DIRECTION 0.0

DETERMINANT 0.47255E-14

CELL NUMBER	ANGLE	CURRENT AMPLITUDE	CURRENT PHASE	CELL NUMBER
1	35.00	8.97951	-122.16	1
2	45.00	3.05661	-114.21	2
3	55.00	1.77597	-114.87	3
4	65.00	0.85976	-123.67	4
5	75.00	0.49555	178.16	5
6	85.00	0.93305	143.93	6
7	95.00	1.41335	144.67	7
8	105.00	1.74348	152.30	8
9	115.00	1.89528	161.23	9
10	125.00	1.88554	169.21	10
11	135.00	1.76117	174.67	11
12	145.00	1.58776	176.50	12
13	155.00	1.43204	174.62	13
14	165.00	1.33522	170.74	14
15	175.00	1.29643	167.79	15
16	185.00	1.29644	167.78	16
17	195.00	1.33520	170.74	17
18	205.00	1.43205	174.62	18
19	215.00	1.58773	176.50	19
20	225.00	1.76118	174.67	20
21	235.00	1.88556	169.21	21
22	245.00	1.89525	161.23	22
23	255.00	1.74348	152.31	23
24	265.00	1.41337	144.67	24
25	275.00	0.93306	143.93	25
26	285.00	0.49554	178.16	26
27	295.00	0.85976	-123.67	27
28	305.00	1.77595	-114.87	28
29	315.00	3.05662	-114.21	29
30	325.00	8.97952	-122.16	30

SLOTTED CYLINDER

KA	2.300	-0.200
APERTURE HALF-ANGLE		30.000
INCIDENT FIELD DIRECTION		0.0

ANGLE	APERTURE FIELDS		AMPLITUDE	PHASE
-28.00	-0.98021	0.64451	1.17312	146.67
-24.00	-1.36907	0.94723	1.66481	145.32
-20.00	-1.66180	1.17919	2.03766	144.64
-16.00	-1.88785	1.36086	2.32721	144.21
-12.00	-2.05832	1.49933	2.54650	143.93
-8.00	-2.17806	1.59731	2.70099	143.74
-4.00	-2.24926	1.65587	2.79304	143.64
0.0	-2.27291	1.67536	2.82364	143.61
4.00	-2.24927	1.65587	2.79305	143.64
8.00	-2.17806	1.59731	2.70099	143.74
12.00	-2.05832	1.49932	2.54649	143.93
16.00	-1.88784	1.36085	2.32720	144.21
20.00	-1.66179	1.17918	2.03765	144.64
24.00	-1.36906	0.94721	1.66479	145.32
28.00	-0.98020	0.64450	1.17310	146.67

DISTANCE	FIELDS ALONG A RADIUS		AMPLITUDE	PHASE
0.0	0.32772	2.98781	3.00572	83.74
1.00	0.20584	3.05992	3.06684	86.15
2.00	0.04669	3.06825	3.06861	89.13
3.00	-0.14866	3.01551	3.01917	92.82
4.00	-0.37864	2.90761	2.93216	97.42
5.00	-0.64144	2.75355	2.82727	103.11
6.00	-0.93482	2.56475	2.72981	110.03
7.00	-1.25507	2.35369	2.66741	118.07
8.00	-1.59489	2.13142	2.66207	126.81
9.00	-1.94090	1.90484	2.71947	135.54
10.00	-2.27291	1.67536	2.82364	143.61